Portland State University
PDXScholar

Physics Faculty Publications and Presentations | Physics

2020

Enhancing Final Image Contrast in Off-Axis Digital Holography using Residual Fringes

Manuel Bedrossian
California Institute of Technology

Kent Wallace
California Institute of Technology

Eugene Serabyn
California Institute of Technology

Chris Lindensmith
California Institute of Technology

Jay Nadeau
Portland State University, jay.nadeau@pdx.edu

Follow this and additional works at: https://pdxscholar.library.pdx.edu/phy_fac

 Part of the Atomic, Molecular and Optical Physics Commons
Let us know how access to this document benefits you.

Citation Details

Bedrossian, M., Wallace, J. K., Serabyn, E., Lindensmith, C., & Nadeau, J. (2020). Enhancing final image contrast in off-axis digital holography using residual fringes. Optics Express, 28(11), 16764-16771.

This Article is brought to you for free and open access. It has been accepted for inclusion in Physics Faculty Publications and Presentations by an authorized administrator of PDXScholar. Please contact us if we can make this document more accessible: pdxscholar@pdx.edu.

Research Article | Vol. 28, No. 11 / 25 May 2020 / Optics Express 16764
Optics EXPRESS

Enhancing final image contrast in off-axis digital holography using residual fringes

MANUEL BEDROSSIAN,[1] J. KENT WALLACE,[2] EUGENE SERABYN,[2] CHRISTIAN LINDENSMITH,[2] AND JAY NADEAU[3,*]

[1]*Department of Medical Engineering, California Institute of Technology, 1200 E. California Blvd, Pasadena CA 91125, USA*
[2]*Jet Propulsion Laboratory, California Institute of Technology, 4800 Oak Grove Dr, Pasadena CA 91011, USA*
[3]*Department of Physics, Portland State University, Portland OR 97201, USA*
[*]*nadeau@pdx.edu*

Abstract: We show that background fringe-pattern subtraction is a useful technique for removing static noise from off-axis holographic reconstructions and can enhance image contrast in volumetric reconstructions by an order of magnitude in the case for instruments with relatively stable fringes. We demonstrate the fundamental principle of this technique and introduce some practical considerations that must be made when implementing this scheme, such as quantifying fringe stability. This work also shows an experimental verification of the background fringe subtraction scheme using various biological samples.

© 2020 Optical Society of America under the terms of the OSA Open Access Publishing Agreement

1. Introduction

Digital off-axis holography is an imaging technique that is capable of capturing both the amplitude and phase of light using a single intensity image (hologram) [1]. It suffers from various types of noise, however, which include but are not limited to photon (shot and speckle) noise, and detector noise (dark noise, read noise, and quantization noise) [2]. Removal of the zero-order and twin-image terms is straightforward in off-axis holography [3,4], and much effort has been devoted to reducing residual noise in holographic reconstructions due to phase aberrations [5,6], astigmatism, spherical aberrations, and anamorphism [7–9]. However, one problem with off-axis holography is slight temporal variations, which make the extended background fringe and speckle pattern difficult to remove to deep levels without the use of computationally expensive methods.

Here we present a computationally inexpensive method of removing the dominant static noise terms from off-axis holographic images. This method involves the background subtraction of raw holograms prior to numerical reconstruction. By only reconstructing the residual localized fringe packets remaining after subtraction of the background fringe pattern [Figs. 1(D)–1(F)], noise contributions such as speckle are removed prior to propagation through the reconstruction process. A theoretical explanation of the approach is presented, as well as practical considerations when implementing this technique. Finally, processing of experimental data from cultures of bacterial and protozoa cells near the resolution limit of the instrument is shown, highlighting this technique's utility.

2. Principle of operation

Figures 1(A) and 1(B) show the optical schematic and laboratory image of a common path DHM instrument described in [10–12], which was used for the experimental data presented in this work. A coherent light source is collimated and passed through two identically sized microfluidic wells. One contains the object of interest while the other contains a reference liquid in order to match optical path lengths with the sample well. The sample and reference beams are then

#394231 https://doi.org/10.1364/OE.394231
Journal © 2020 Received 1 Apr 2020; revised 30 Apr 2020; accepted 30 Apr 2020; published 19 May 2020

Optics EXPRESS

passed through two separate but identical objective lenses. Finally, a relay lens recombines the beams at a detector plane, creating an interferogram (hologram).

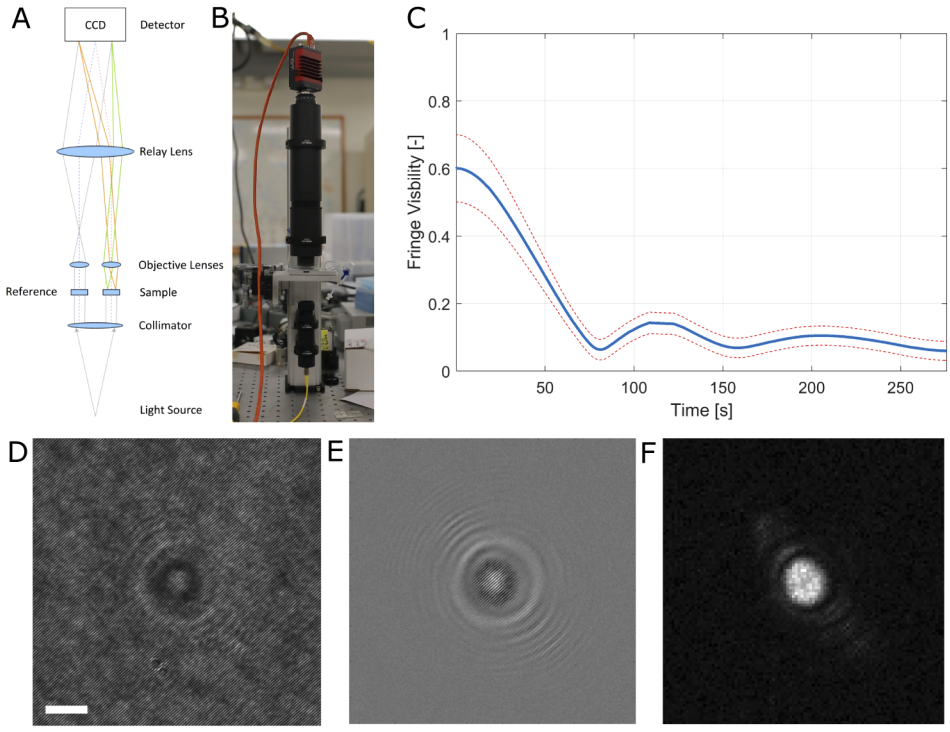

Fig. 1. Optical Schematic of the DHM instrument used throughout this work (A), an image of the benchtop instrument (B), and fringe stability of the DHM instrument as a function of time (C). Centerline indicates the mean fringe visibility and dashed lines indicate the 95% confidence interval range. (D) Raw hologram with a single *B. subtilis* bacterium in the field of view. (E) The same hologram after background subtraction and (F) a map of local fringe visibility of the background subtracted hologram in E, showing the residual localized fringe packets of dynamic objects. Scale bar in D represents 10 μm for D, E, and F.

Let two monochromatic and coherent beams, $0(x,y,t)$ and $R(x,y)$ corresponding to object and reference beams, respectively, be incident on an optical detector, such that the resulting interference pattern recorded by the digital detector is

$$I[x_d, y_d, nT] = (O + R)(O + R)^* = |O|^2 + |R|^2 + RO^* + R^*O, \tag{1}$$

where x_d, y_d are discrete spatial coordinates within the hologram, n is an integer value describing a discrete time sample of the intensity incident on a digital detector at a sampling interval of T seconds. Because relative phase shifts occur between beams, unstable fringe phases can in fact be taken into account by attributing them entirely to the object beam, with the reference beam assumed ideal. The object beam can be expressed as the superposition of a temporally static beam $O_s(x,y)$ and spatiotemporal deviations from that static beam caused by dynamic objects $\varepsilon(x, y, t)$, such that$O(x, y, t) = O_s(x, y) + \varepsilon(x, y, t)$. Thus, the hologram can be expressed as

$$I[x_d, y_d, nT] = |O_s|^2 + |\varepsilon|^2 + |R|^2 + RO_s^* + R^*O_s + (O_s + R)\varepsilon^* + (O_s + R)^*\varepsilon. \tag{2}$$

The temporally averaged hologram is defined as

$$\bar{I}[x_d, y_d] = |O_s|^2 + |\bar{\varepsilon}|^{\bar{2}} + |R|^2 + RO_s^* + R^*O_s + (O_s + R)\bar{\varepsilon}^* + (O_s + R)^*\bar{\varepsilon}. \tag{3}$$

Optics EXPRESS

For a sufficiently large timescale, it can be assumed that. $\bar{\varepsilon} = 0$ The residual hologram is defined as the difference between Eqs. (2) and (3):

$$I_R[x_d, y_d, nT] = I - \bar{I} = O_s\varepsilon^* O_s^*\varepsilon + R\varepsilon^* + R^*\varepsilon + |\varepsilon|^2 - |\bar{\varepsilon}|^2. \quad (4)$$

The O_s and ε beams are on-axis with each other and thus their interference terms only contribute to the zero-order term of Eqs. (3) and (4). The term $|\varepsilon|^2 - |\bar{\varepsilon}|^2$ is also a zero-order term. The residual hologram in Eq. (4) is then binned and quantized into an 8-bit format in order to be compatible with other downstream image processing software. Using typical techniques of Fourier-space spatial filtering, which removes zero-order and twin image artifacts from the reconstructed images [3], the spatially filtered hologram that becomes reconstructed can be expressed as $I_R^F = R^*\varepsilon$.

3. Practical considerations

Background subtraction of holograms is useful because any stationary artifacts in the image become attenuated, leaving only dynamic objects. If the background fringes of the hologram are stable, these fringes would be effectively removed from the resulting image, except for localized fringe 'packets' associated with any particle that has moved through the field of view of the hologram. Figure 1(D) shows a typical raw hologram with a single *B. subtilis* bacterium in the center of the field of view. Figure 1(E) shows the same hologram after background subtraction and Fig. 1(F) shows the background subtracted hologram as a function of local fringe visibility [see Eq. (5)]. Figures 1(E) and 1(F) show that after background subtraction, only localized fringe packets pertaining to dynamic particles remain in the residual hologram. This background subtraction technique vastly increases the signal to noise ratio of any dynamic particle in an image sequence, making it much easier for automated particle detection algorithm to detect particles of interest in space and time. We show here that rapid motion is not necessary for the method to work; movement as small as bacterial Brownian motion will suffice.

Such a background subtraction technique requires a stable interferometer. Many sources of noise can introduce shifts in DHM fringes, causing them to drift across the field of view of the detector. These noise sources include but are not limited to speckle noise, temporal phase noise caused by uncorrelated variations between the two beams of the instrument, as well as changes in illumination wavelength from instabilities in the illumination source. These sources of noise introduce an upper limit on the timescales where the proposed background subtraction scheme is useful. As the background fringes shift, they will by definition become dynamic objects in the image, thus no longer being removed by the background subtraction scheme.

The data used here were taken with a common-path off-axis DHM described previously [10], or by a multi-wavelength version permitting simultaneous capture at 3 wavelengths [12], with parameters in Table 1. The valid timescales of this background subtraction technique, with this relatively stable instrument, were quantified by collecting holographic images as a function of time without a sample in the field of view of the instrument. Temporally averaged holograms were calculated at various timescales through the hologram sequence. Fringe stability was inferred by calculating the average fringe visibility of the temporally averaged hologram. This is possible because if the fringes are absolutely stable (static), the temporally averaged hologram would equal the fringe pattern of each hologram in the sequence. As the fringe pattern begins to shift, they will become dynamic artifacts in the image and thus not appear in the temporally averaged hologram. Figure 1(C) shows a plot of fringe stability as a function of time for the DHM instrument used throughout this work. The center line in the plot signifies the mean fringe visibility value while the dotted lines signify the 95% confidence interval value range. By defining the point of fringe decorrelation as the point in time when the fringe visibility decreases by -3 dB, the upper timescale that should be used for this background subtraction scheme using

Optics EXPRESS

our common mode instrument is roughly 40 seconds. Much shorter decorrelation times are expected for less stable instruments.

Table 1. Properties of the common path DHM instrument.

Property	Value [unit]
Operating wavelengths	405 [nm]
	520 [nm]
	685 [nm]
Numerical aperture	0.38 [-]
System magnification	19.7 [-]
Lateral resolution	0.7 [μm]

The average fringe visibility of a temporally averaged hologram was calculated by the distinct block processing of the temporally averaged hologram, where each distinct block is an m by n non-overlapping submatrix within the hologram. The size of these distinct blocks correspond to a single spatial period of the fringes within the hologram. The fringe visibility of the $(i,j)^{\text{th}}$ block was calculated such that

$$V_{i,j} = \frac{I_{\max} - I_{\min}}{I_{\max} + I_{\min}}, \tag{5}$$

where I_{max} and $I_{\min}$ are the maximum and minimum pixel value within the $(i,j)^{\text{th}}$ block. The mean fringe visibility value across all distinct blocks can then be calculated and becomes the average fringe visibility for that particular temporally averaged hologram.

In addition to an upper limit on the timescale where this background subtraction scheme is useful, it is important to note a lower limit as well. Depending on the particulate speed, a large enough time scale must be used to allow significant positional shifts. This method was found to be sensitive enough to capture the small Brownian motion of bacterial cells.

It is possible to conduct this proposed background subtraction method using a median calculated hologram. Using the median is an alternative that was also explored, but made no difference in this case, given the low variability between the individual holograms on the timescales used in this work. This is advantageous given the much lower computational overhead associated with a mean calculation as a oppose to a median calculation.

4. Experimental procedure

The DHM was used to image two strains of bacteria (*Bacillus subtilis* and *Vibrio alginolyticus*), as well as the protozoan, *Euglena gracilis*. A 1 mm deep well was filled with a dilution of the biological sample in minimal media. A 'motility' medium was used for *B. subtilis* which would not harm the organisms but hinder their growth (10 mM phosphate buffer pH 7.4, 10 mM NaCl, 0.1 mM EDTA, 0.1 mM glucose). Due to the marine origins of *V. alginolyticus*, a different minimal media recipe was used (50 mM Tris buffer, 300 mM NaCl, 5 mM $MgCl_2$, 5 mM glucose). *E. gracilis* was diluted in spring water. Holographic images were recorded at a frame rate of 15 frames per second. Background image subtraction was performed with a timescale of 10 seconds (150 holograms). Both the raw holograms and background subtracted holograms were then spatially filtered and reconstructed via the angular spectrum method using either the commercial software KOALA (Lyncée Tec SA, www.lynceetec.com) or a Fiji-based plug-in developed by our group [3,13,14]. All bacterial data were recorded using a monochromatic 405 nm laser illumination source. DHM images of *E. gracilis* were acquired using the multi-wavelength implementation of the common path DHM instrument, using a 405, 520, and 685 nm laser illumination source simultaneously.

Optics EXPRESS

5. Results

Figure 2 shows a raw hologram and background-subtracted hologram of a single *B. subtilis* bacterium [Figs. 2(A) and 2(B), respectively] and their respective Fourier spectra [Figs. 2(C) and 2(D)]. Figures 2(E) and 2(F) show the intensity reconstruction of the same bacterium using the raw hologram and background subtracted hologram, respectively. Figure 2(G) shows a single plane intensity reconstruction of a motile *B. subtilis* bacterium over roughly two seconds. This image is a composite image rendered by the minimum pixel intensity projection of multiple time points and illustrates the organism's motion through time. Figures 2(H) and 2(I) show vertical line plots of pixel values through the bacterium for both the raw reconstruction and background subtracted reconstruction [Figs. 2(G) and 2(H), respectively]. Employing the background subtraction technique on data sets containing *B. subtilis* saw an increase in SNR of roughly an order of magnitude (11x improvement in SNR)

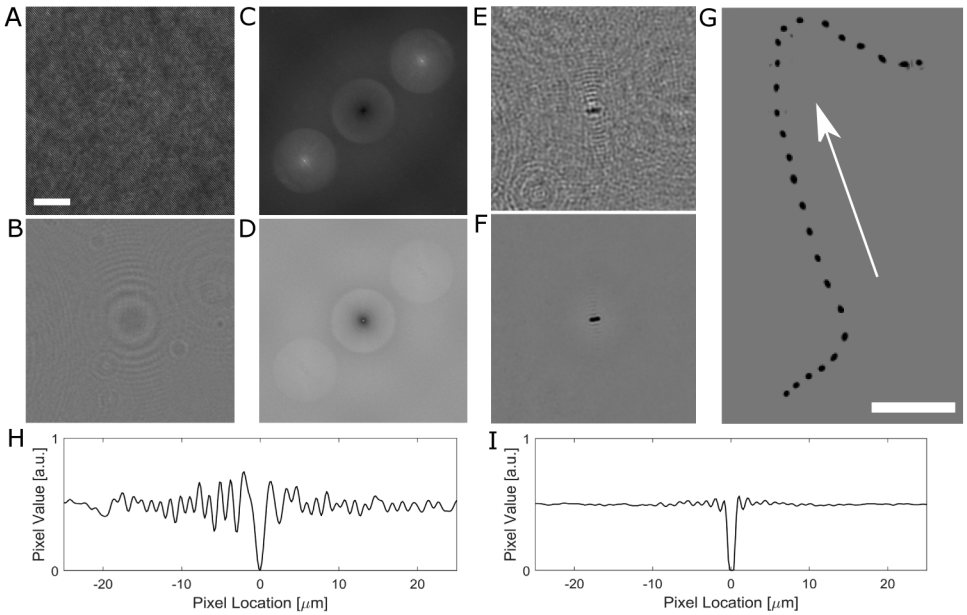

Fig. 2. Raw hologram of sample containing *B. subtilis* (A), the identical hologram after background subtraction (B), and their respective Fourier spectra (C and D). Intensity reconstruction of the same *B. subtilis* bacterium without (E) and with (F) the use of the residual fringe visibility analysis. (G) Select trajectory of a motile *B. subtilis* bacterium. This image is a composite image rendered by the minimum pixel intensity projection of 2 seconds of data. Arrow indicates the direction of motion. (H and I) Vertical line plots of pixel values through the bacterium shown in E and F, respectively. Scale bar in A represents 10 μm for A, B, E, and F. Scale bar in G represents 10 μm.

Figure 3 shows a raw and background subtracted hologram of a select *V. alginolyticus* bacterium [Figs. 3(A) and 3(B), respectively], and their respective Fourier spectra [Figs. 3(C) and 3(D)]. Figures 3(E) and 3(F) show a single plane intensity reconstruction of the same hologram from Figs. 3(A) and 3(B), respectively. These intensity reconstructions also demonstrate an order of magnitude increase in SNR. Figures 3(G) and 3(H) show a volumetric rendering of intensity reconstructions using the raw and background subtracted holograms, respectively. These volumetric renderings have been thresholded to the same value for comparison. The implementation of the background subtraction technique can be seen to increase the SNR of volumetric intensity reconstructions which can allow for the 3D localization of near diffraction

Optics EXPRESS

limited objects such as *V. alginolyticus*. Due to the standard thresholding used in the volumetric renderings of Figs. 3(G) and 3(H), vertical lines can be seen in Fig. 3(G), which are the residual artifacts of the point spread function of the *V. alginolyticus*. Downstream processing techniques, such as deconvolution, would be effective in removing such artifacts.

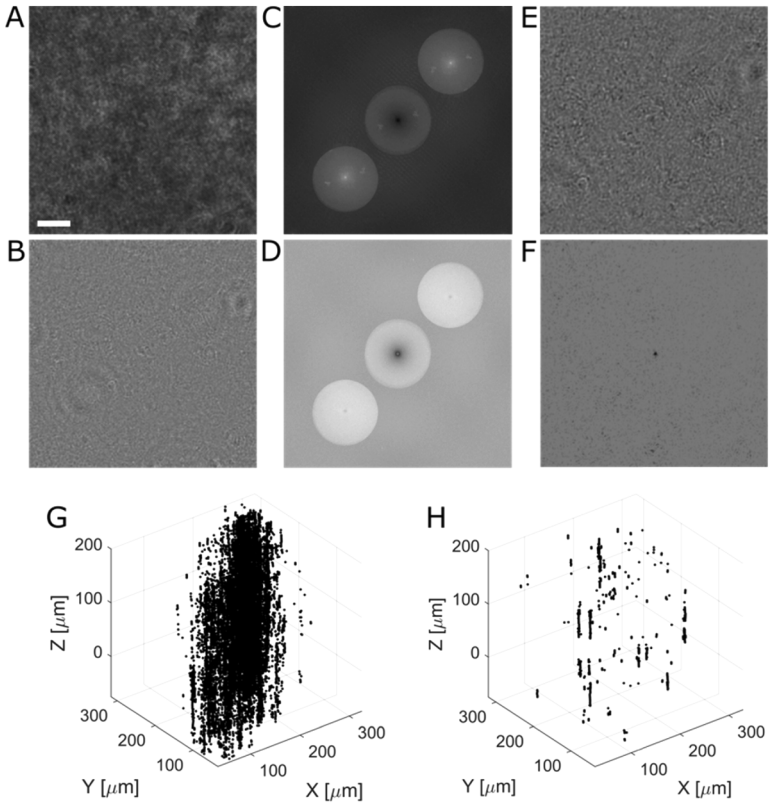

Fig. 3. Raw hologram of *V. alginolyticus* (A), the identical hologram after background subtraction (B), and their respective Fourier Spectra (C and D). Intensity reconstruction of the same *V. alginolyticus* bacterium without (E), and with (F) the use of the residual fringe visibility analysis, and a 3D rendering of the reconstructed intensity z-stack of the raw (G) and background subtracted hologram (H). Scale bar represents 10 μm for (A, B, E, and F).

Figure 4 shows a raw and background subtracted hologram of multi-wavelength DHM data containing *E. gracilis* [Figs. 4(A) and 4(B)], and their respective Fourier spectra [Figs. 4(B) and 4(C)]. Figures 4(D) and 4(E) show a pseudo-colored composite intensity reconstructed image of a select *E. gracilis* using the raw and background subtracted hologram, respectively. The use of background subtracted holograms for multi-wavelength DHM data dramatically reduces the need for other post-processing unique to multi-wavelength data such as white balancing. Furthermore, the reduction in noise enables sub-cellular features of the *E. gracilis* to be much more visible, namely, the stigma (eyespot) and nucleus.

Optics EXPRESS

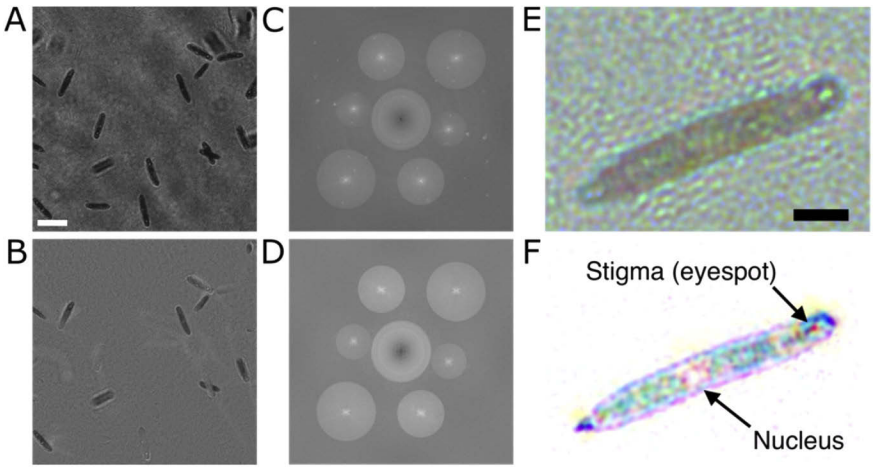

Fig. 4. Raw multiwavelength hologram of sample containing *E. gracilis* (A), the identical hologram after background subtraction (B), as well as their respective spectra (C and D, respectively). A pseudo-colored composite intensity reconstruction of a select *E. gracilis* using the raw hologram (E), and background fringe subtraction technique (F). Scale bar in (A) represents 50 μm for both (A and B). Scale bar in (E) represents 20 μm for both (E and F).

6. Conclusion

A novel method of enhancing image contrast of intensity reconstructions of digital off-axis holographic images is presented, including a theoretical justification, practical considerations in its implementation, and an experimental verification using biological samples. With roughly an order of magnitude of increased contrast provided by this method, standard image thresholding and clustering techniques become possible and enable high throughput and low computational overheard volumetric tracking. Furthermore, by conducting background subtraction on the raw holograms as opposed to the volumetric reconstruction, computational overhead is reduced proportionally to the number of axial planes reconstructed, potentially significantly decreasing computation times.

It is critical to note that fringe stability is necessary for this approach to work. We implemented it using a common-path off-axis DHM designed to be stable against vibrations. With a traditional Mach-Zehnder interferometer, the fringes may not be stable on the timescales reported in this work. Thus, the fringe stability and resultant number of frames used for background fringe subtraction will need to be determined for each instrument and light source combination.

Funding

Jet Propulsion Laboratory.

Disclosures

The authors declare no conflicts of interest.

References

1. M. K. Kim, L. Yu, and C. J. Mann, "Interference techniques in digital holography," J. Opt. A: Pure Appl. Opt. **8**(7), S518–S523 (2006).
2. M. Bedrossian, J. Nadeau, E. Serabyn, and C. Lindensmith, "Sources and propagation of errors in quantitative phase imaging techniques using optical interferometry," in *Quantitative Phase Imaging III*. 2017. International Society for Optics and Photonics.

Optics EXPRESS

3. E. Cuche, P. Marquet, and C. Depeursinge, "Spatial filtering for zero-order and twin-image elimination in digital off-axis holography," Appl. Opt. **39**(23), 4070–4075 (2000).
4. N. Demoli, J. Meštrović, and I. Sović, "Subtraction digital holography," Appl. Opt. **42**(5), 798–804 (2003).
5. T. Colomb, J. Kuhn, F. Charriere, C. Depeursinge, P. Marguet, and N. Aspert, "Total aberrations compensation in digital holographic microscopy with a reference conjugated hologram," Opt. Express **14**(10), 4300–4306 (2006).
6. A. T. Khmaladze, R. L. Matz, J. Jasensky, E. Seeley, M. M. Banaszak Holl, and Z. Chen, "Dual-wavelength digital holographic imaging with phase background subtraction," Opt. Eng. **51**(5), 055801 (2012).
7. S. De Nicola, A. Finizio, G. Pierattini, P. Ferraro, and D. Alfieri, "Angular spectrum method with correction of anamorphism for numerical reconstruction of digital holograms on tilted planes," Opt. Express **13**(24), 9935–9940 (2005).
8. S. Grilli, P. Ferraro, S. De Nicola, A. Finizio, G. Pierattini, and R. Meucci, "Whole optical wavefields reconstruction by digital holography," Opt. Express **9**(6), 294–302 (2001).
9. A. Stadelmaier and J. H. Massig, "Compensation of lens aberrations in digital holography," Opt. Lett. **25**(22), 1630–1632 (2000).
10. J. K. Wallace, S. Rider, E. Serabyn, J. Kuhn, K. Liewer, J. Deming, G. Showalter, C. Lindensmith, and J. Nadeau, "Robust, compact implementation of an off-axis digital holographic microscope," Opt. Express **23**(13), 17367–17378 (2015).
11. C. A. Lindensmith, S. Rider, M. Bedrossian, J. Kent Wallace, E. Serabyn, G. Max Showalter, J. W. Deming, and J. Nadeau, "A submersible, off-axis holographic microscope for detection of microbial motility and morphology in aqueous and icy environments," PLoS One **11**(1), e0147700 (2016).
12. J. K. Wallace, E. Serabyn, C. Lindensmith, J. Nadeau, S. Rider, and M. Bedrossian, "A multiwavelength digital holographic microscope architecture for enhancing life detection," *2019 IEEE Aerospace Conference*, Big Sky, MT, USA, 2019, pp. 1–6.
13. D. Cohoe, I. Hanczarek, J. Kent Wallace, and J. Nadeau, "Multiwavelength digital holographic imaging and phase unwrapping of protozoa using custom Fiji plug-ins," Front. Phys. **7**, 94 (2019).
14. J. Schindelin, I. Arganda-Carreras, E. Frise, V. Kaynig, M. Longair, T. Pietzsch, S. Preibisch, C. Rueden, S. Saalfeld, B. Schmid, J.-Y. Tinevez, D. J. White, V. Hartenstein, K. Eliceiri, P. Tomanak, and A. Cardona, "Fiji: an open-source platform for biological-image analysis," Nat. Methods **9**(7), 676–682 (2012).

131.252.181.105 {ts '2020-07-16 18:51:46'}